PAPER

Gigahertz acoustic vibrations of Ga-doped ZnO nanoparticle array

View the article online for updates and enhancements.

IOP ebooks™

Bringing you innovative digital publishing with leading voices to create your essential collection of books in STEM research.

Start exploring the collection - download the first chapter of every title for free.

Gigahertz acoustic vibrations of Ga-doped ZnO nanoparticle array

Dickson Mwenda Kinyua[1] , **Hua Long**[1] , **Xiangyuan Xing**[1],
Stephen Njoroge[1] , **Kai Wang**[1], **Bing Wang**[1] **and Peixiang Lu**[1,2]

[1] Wuhan National Laboratory for Optoelectronics (WNLO) and School of Physics, Huazhong University of Science and Technology, Wuhan 430074, People's Republic of China
[2] Hubei Key Laboratory of Optical information and Pattern Recognition, Wuhan Institute of Technology, Wuhan 430074, People's Republic of China

E-mail: longhua@hust.edu.cn

Abstract

In this work, we present an experimental study on the acoustic vibrations of ZnO nanoparticles array with different concentration of Ga dopings by using femtosecond pump-probe technique. The Ga-doped ZnO (GZO) nano-triangle particles with the sizes of 190, 232 and 348 nm are fabricated by nanosphere lithography and pulsed laser deposition method. The result indicates that the frequency of acoustic vibrations of GZO nanoparticles decrease as the Ga-concentration is increased. Importantly, the vibration period of the GZO nanoparticles at the same Ga doping concentration show a nonlinear increase as the nanoparticle size is increased, which is different from the common linear dependency in undoped ZnO nanoparticles. It may be attributed to the crystal structure distortion and elastic characteristics variation due to Ga doping, and the elastic modulus at 7.3% Ga doping is decreased by 30%–60% for GZO nanoparticles with different sizes. The study can be very helpful for evaluating the crystal structure distortion and elastic characteristics of doped nano-materials with optical methods. Besides, it can offer a complementary method of thermal management in ZnO based optoelectronic devices.

Keywords: GZO, acoustic vibrations, nanoparticle arrays, crystal structure distortion

(Some figures may appear in colour only in the online journal)

1. Introduction

The interest in ZnO nanostructures continues to grow due to its unique properties that make them attractive for application in nano-devices. ZnO has a wide bandgap, large exciton binding energy (60 meV) at room temperature [1], is biosafe and biocompatible [2]. It is used in various photonic devices such as LEDs, lasers and room temperature polariton lasers [3–5]. To further enhance the performance of the ZnO nano-devices, the material is often doped to alter the intrinsic properties. Various dopants such Mg [6], N [7], Al [8] and Ga [9–11] have been used, but Ga offers various advantage such as: close atomic radius of Ga and Zn, leading to minimal strain and local lattice distortion [12, 13] and increased transparency in the visible region [14]. However, much of the work done on the effect of Ga doping of ZnO (GZO) is based on static techniques such as UV–vis, Raman and x-ray.

Therefore, it is necessary to study the dynamic properties of GZO to determine the carrier's behavior such as electron–phonon interactions, and their effect on materials properties.

Pump-probe spectroscopy is a powerful time-resolved approach for studying excited state dynamics in nano-materials owing to its high temporal resolution [15]. The pump laser excite the carriers in materials. Then energy relaxation and electron–phonon interaction leads to some strain in the materials, which is monitored by probe laser. It has been widely used to study the dynamics of coherent phonons in various material systems, including metals, semiconductors and heterostructure forms [16–18]. Specifically, it has also been used to characteristic the coherent acoustic phonons (CAP) in c-ZnO epitaxial film [19] and the interaction of CAPs and polariton states in 0.5 mm thick c-ZnO single crystal [20]. Additionally, pump-probe spectroscopy has become a key to non-destructive apprehension of the

mechanical properties in nanostructures [21–23]. This all-optical time-resolved method is also among the go-to techniques to characterize interfacial thermal transport at the nanoscale, which is important for optoelectronic nanodevices.

So far, a lot of research work about the coherent acoustic vibrations have been done on the effects of periodic modifications of nanostructures. Moreover, a variety of factors can also influence the vibrations, such as type of substrate [24–26], periodicity of the nanoparticles, aspect ratio and so on [27]. In fact, doping in the nanomaterials can also lead to influence on the acoustic vibrations due to the crystal structure distortion and elastic properties change. However, the effect of doping on the coherent vibrations of nanostructures is seldomly reported. Herein, for the first time we report a detailed study on the influences of Ga doping on the acoustic vibration in GZO nanoparticle arrays by using femtosecond pump-probe technique. It indicates that the frequency of acoustic vibrations of GZO nanoparticles decrease as the Ga-concentration is increased. Importantly, the vibration period of the GZO nanoparticles at the same Ga doping concentration show a nonlinear increase as the nanoparticle size is increased, which is different from the common linear dependency in undoped ZnO nanoparticles. It may be attributed to the crystal structure distortion and elastic characteristics variation due to Ga doping, and the elastic modulus at 7.3% Ga doping is decreased by 30%–60% for GZO nanoparticles with different sizes. The study can be very helpful for evaluating the crystal structure distortion and elastic characteristics of doped nano-materials with optical methods. Besides, it can offer complementary way of thermal management in ZnO based optoelectronic devices.

2. Experimental details

The GZO nano-arrays were fabricated on mask templates by pulsed laser deposition (PLD) method with KrF excimer laser (Lambda Physics, 330 mJ, 248 nm repetition rates of 5 Hz). GZO films were also deposited on silicon substrates under the same condition to compare with the nano-triangle particle arrays [13]. The mask templates for nano-arrays were prepared on the cleaned substrates using polystyrene spheres with diameter of 820, 1000 and 1500 nm (Duke Scientific Corporation) by nanosphere lithography (NSL) method. After the deposition by PLD, the samples were ultra-sonicated in alcohol for 30 s to clean up the polystyrene spheres and GZO nano-arrays were obtained. To get arrays or films with different doping level, GZO targets of different doping concentration (0%, 2.9%, 5.0% and 7.3%) were used in PLD processing. The GZO targets were fabricated by standard solid state reaction method using specific amount of ZnO (99.99%) and Ga_2O_3 (99.99%). The surface morphologies and crystal structure of the GZO nano-arrays and films were measured by atomic force microscope (AFM, Veco Nano-Scope MultiMode) and x-ray diffraction (XRD, Empyrean, PANalytical B.V.), respectively. The UV–visible transmission spectra were performed by UV–visible spectrophotometer (HITACHI U3310).

A home-built pump-probe experimental system was used to measure the transient reflectivity change $\Delta R/R$ of the samples. A regeneratively amplified Ti-sapphire femtosecond laser centered at 800 nm (Astrella, Coherent, 35 fs and 1 kHz) was used as the source pulse, with a mode-locked Ti-sapphire femtosecond laser as seed laser [28]. The pump wavelength is 400 nm, generated by a second harmonic BBO crystal, and was focused through an 8 cm lens onto the surface of the GZO films or nano-arrays. The probe wavelength is 800 nm, which is delayed in time to the pump and is focused onto the same position of the sample through an objective lens (20×). To collect the reflected probe beam from the sample surface, a balanced photodiode detector (Thorlabs, PDB210A/M) connected by a lock-in amplifier (Stanford, SR830) is used.

3. Results and discussion

Figures 1(a)–(c) show AFM images of GZO nanoparticle arrays. The figures indicate uniformly distributed periodic nano-triangle particles. The bisector lengths of the nano-triangles were about 190 nm, 232 nm and 348 nm, respectively. AFM images of the ZnO nano-film at different Ga doping levels of 0%, 2.9% and 7.3% are shown in figures 1(d)–(f), respectively. The images show smooth surface in all the samples. The RMS of the nano-film reduced from 17.6 to 2.9 nm with Ga doping concentrations increased from 0% to 7.3%.

To determine the crystal structure distortion in ZnO introduced by Ga doping, we compare the XRD patterns of GZO at different Ga doping concentrations, see figure 2(a). The results revealed that all the samples have a sharp peak at $2\theta = 34.460°$, corresponding to ZnO (002) plane. This implies that the samples maintain the hexagonal wurtzite crystal structure. For the 7.3% Ga^{2+} doped sample, (110), (100) and (101) crystal planes are also observed though (002) plane remains superior. Besides, it was observed that the (002) peak position shifted from 34.460° to lower values with increase in Ga concentrations, as shown in table 1. This indicates relative strain in ZnO nano-arrays due to Gallium doping [29].

Additionally, we obtained the change in full wave half maximum (FWHM), and the average crystalline size (D_{hkl}) as doping levels was increased, (where the change in FWHM and D is defined as $FWHW/D_{hkl(\text{Ga doped GZO})} - FWHD/D_{hkl(0\% \text{ doped GZO})}$). Table 1 show that the FWHM increases with increasing Ga concentration, meaning that the crystalline size reduced. The crystalline size of the GZO nano-film can be calculated using Debye Scherer equation [30] $[D_{hkl} = k\lambda/(\beta\cos\theta_{hkl})]$ where k is a constant ($k = 0.89$), λ is the wavelength of XRD with Cu-Kα radiation ($\lambda = 0.154\,06$ nm) and β is the FWHM in radians of the (002) diffraction peak. From the table it is concluded that increasing the Ga contents leads to decrease in D_{hkl}. Besides, we calculate the internal strain (ε) introduced in the crystal using
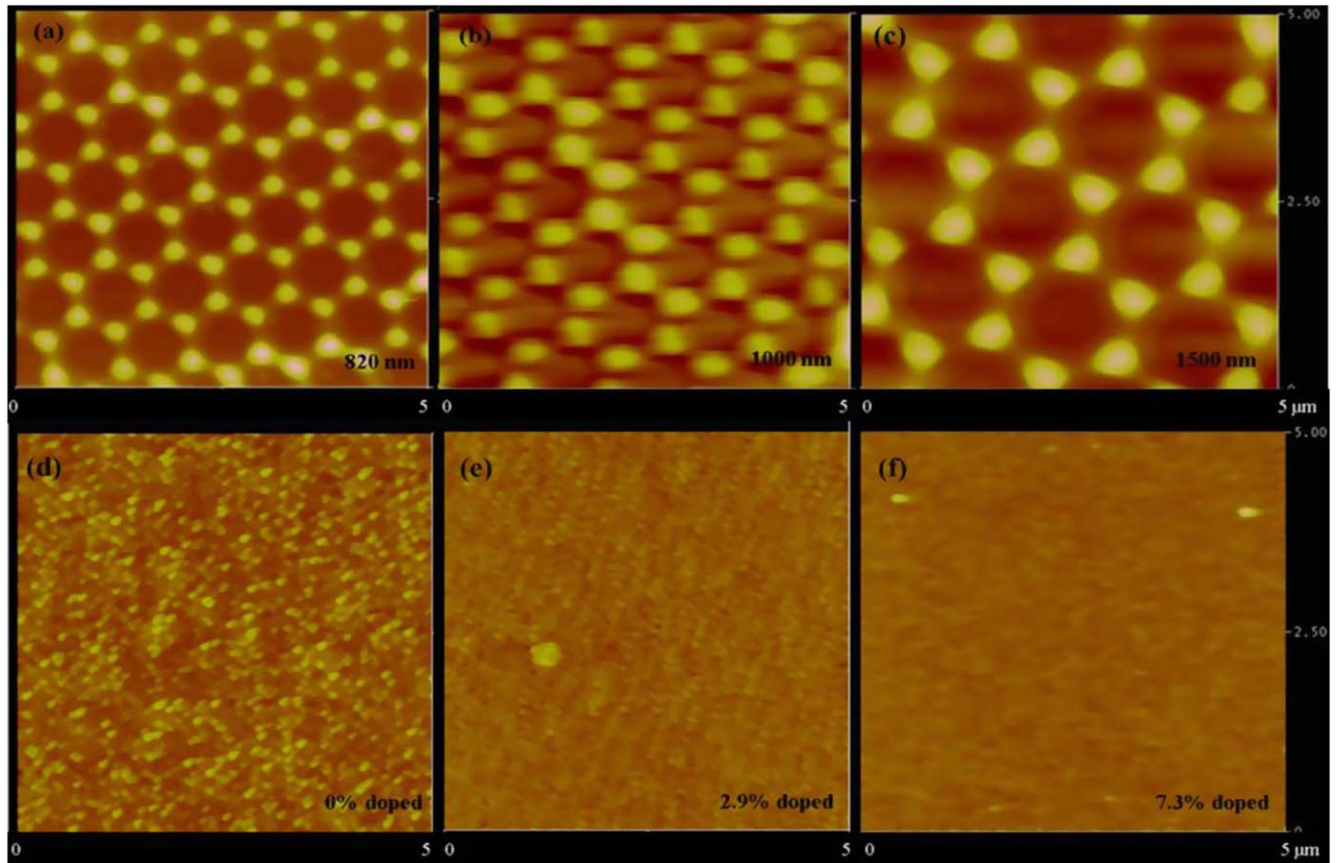
Figure 1. AFM images of GZO nanostructures; (a)–(c) are nano-particle arrays prepared with polystyrene spheres of diameters 820 nm, 1000 nm and 1500 nm respectively. While (d)–(f) are the nano-films at 0%, 2.9% and 7.3% Ga doping respectively.
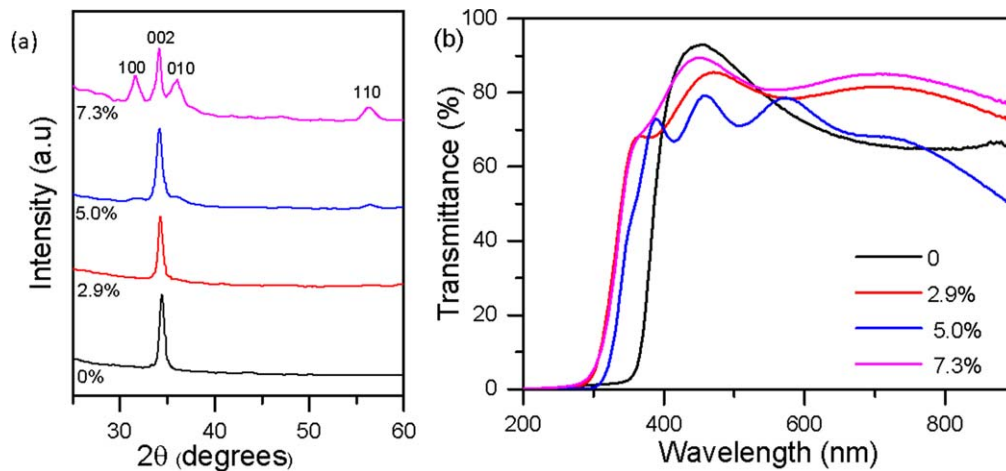
Figure 2. XRD of GZO nanoparticle arrays deposited at different Ga concentration which shows preferential orientation along (002) plane. (b) UV–visible transmission spectra for GZO nanoparticle arrays at various Ga concentration.

the expression:

$$\varepsilon = \frac{\beta}{4 \tan \theta}, \tag{1}$$

where β is the FWHM and θ is the diffraction angle [31]. The calculation results show increased strain in the films with increasing Ga concentration (see table 1).

Figure 2(b) shows the UV–visible transmission spectra of the GZO arrays deposited at different concentrations of Ga in

200–900 nm range. All the spectra show a sharp absorption edge in the region between 300 and 400 nm, which shifts depending on the doping. The shifting of the absorption edges could have been caused by doping induced Burstein–Moss effect. Similar results were obtained for GZO films deposited by spray pyrolysis [32].

In the pump-probe spectroscopy experiments, to observe the change in the acoustic vibrations in GZO nanoparticles, 400 nm pump laser beam was used to excite the electrons

Table 1. 2θ, change in FWHM and D_{hkl}, and ε of GZO nano-film.

Doping level (%)	2θ peak position (°)	Change in FWHM (°) 10^{-2}	Change in D_{hkl} (nm)	Internal strain $\varepsilon \times 10^{-3}$
0	34.460	—	—	4.705
2.9	34.227	0.650	−0.4669	4.830
5.0	34.159	3.863	−2.5643	5.298
7.3	34.094	6.225	−3.8703	5.645

*The negative in D_{hkl} suggests smaller D_{hkl} value to undoped sample.

from the valence band to the conduction band by two photon absorption (TPA) or one photon absorption via the deep levels such as Zn-interstitials and Zn-vacancies [33]. Additionally, acoustic phonons may be induced by thermal and electronic stress created by pump pulse. Figures 3(a)–(c) show the differential reflectance ($-\Delta R/R$) traces upon exciting the GZO nano arrays with different sizes at 2.9% of Ga concentration. Since the single photon energy of the pump laser was below the band gap E_g of ZnO, there is a small dip around the zero decay time attributed to TPA [34]. The TPA was followed by an immediate positive turn which is attributed to band filling effect. Finally, through the electron–phonon scattering thermalization and other relaxation mechanisms, the excited electrons decay exponentially. Interestingly, there was a dip on the decay for the undoped arrays as shown by an arrow in figure 3(d) because of band-gap renormalization (BGR) effects [35]. However, Ga doping concentration increasing in ZnO particles results in surface defects increasing [36] and therefore may induce the diminished effect of the BGR.

The $-\Delta R/R$ can be expressed as a complex product of the Gaussian function [($g(t)$] and a multi-decay function (M_T) as follows $-\Delta R/R = g(t) \otimes M_T$ [37]. M_T is the sum of the electronic and phonon relaxation contribution. We first study the electronic relaxation effects (R_e) as a result of doping. The red continuous line in figure 3 shows the fitting of the R_e by the below formula [38]:

$$R_e = A_1 \exp(t/\tau_1) + A_2 \exp(t/\tau_2) \\ + A_3 \exp(t/\tau_3) \qquad (2)$$

A_1, A_2 and A_3 are the scaling factors whereas, τ_1, τ_2 and τ_3 represents the ultrafast, fast and slow lifetime constants respectively. The ultrafast and fast process can be attributed to the recombination of carriers at the defects. The slow decay could be set down to electron–phonon coupling and electron–hole recombination. Similar result was obtained for Molybdenum doped ZnO nanocrystalline thin films [39] and aluminum doped ZnO thin films [31].

To investigate the acoustic vibration in GZO nanoparticle arrays, we separate the background contribution of the excitons in the nanoparticles to obtain the residual traces, see the insert in figures 3(a)–(d). After applying a fast Fourier transform (FFT), a spectrum with a distinctive peak frequency for each array is obtained as shown in figures 4(a) and (b) for undoped and 7.3% doped GZO respectively. The black, red and blue represent the 190 nm, 232 nm and 348 nm particles

respectively. There is a decrease in frequency as the particles size become larger for all doping concetrations. The vibrations in the nanotriangles can be attributed to radial breathing modes (*f inversely proportional to particle size*) and edge modes along the boundaries [40]. Figure 4(c) shows the relationship between the nano-triangle particle size and the periodic time of the acoustic vibration at various doping concentrations. The periodic time of the vibrations increased with the array size.

For the undoped ZnO nanoparticles, the dotted line shows the linear fitting, see in figure 4(c). We note that the line passes through zero which indicates the propagation stress from silicon substrate does not impact the vibrations oscillation [18]. The frequency of the nano-triangle arrays can be defined as follows [41, 42]:

$$\frac{1}{f} = \frac{2a}{v}, \qquad (3)$$

where f is the frequency, v is the longitudinal sound velocity in bulk and a is bisector length of the triangular nano-arrays. Comparing the equation (3) and linear fit ($T = 3.3775a \times 10^{-4}$), a longitudinal sound velocity of $5921.5 \pm 90 \, \text{ms}^{-1}$ is obtained from the gradient. This is slightly lower than the velocity in bulk ZnO [19]. This demonstrate the effect of periodic boundary conditions on the phonon dispersion using triangular nanoparticles. Using relations $V_S = \sqrt{C/\rho}$ [43] where $v_s = 5921.5 \pm 90 \, \text{ms}^{-1}$ is longitudinal sound velocity, C is the elasticity and $\rho = 5606 \, \text{kg m}^{-3}$ is the mass density for ZnO. We obtain a elasticity value of 196.6 ± 6 GPa which is within 111.2 ± 4.7 GPa and 310 ± 40 GPa for single crystal [44] and epitaxial layers [45] ZnO respectively using spherical nanoindentation.

However, once the dopants are introduced, the vibration period show an unusual nonlinear increase with the particle size increase, for GZO arrays of the same doping concentration (figure 4(c)). Several factors such as the periodicity of the nanoparticles and the substrate effect can contribute to this nonlinear effect as pointed in the introduction. However, since all the samples were prepared under the same experimental conditions, we conclude that the effect of doping had a major impact on the unusual change of vibration period in our experiments. We suggest that for the GZO nanotriangles with larger size which have higher aspect ratio, the possible frequency shift contributed from surface acoustics effects [27], might be increased with the doping effect. As earlier discussed, Ga-doping introduced distortions and strain in the crystal structure of ZnO could account for the variations that are observed in these doped nano-triangle array samples. Figure 4(d) shows that the elasticity (C) value decreased with increase in Ga concetration and size of the nano arrays. This is mainly attributted to the corresponding reduction in the vibration frequency as both the Ga concetration increased and array size become bigger.

To verify that indeed the frequency of the acoustic vibrations in ZnO is affected by crystal distortions as a result of Ga doping, we measured the time-resolved spectroscopy of the GZO nano-films deposited under the same condition. Figure 5(a) shows the FFT graph of the nano-films at different
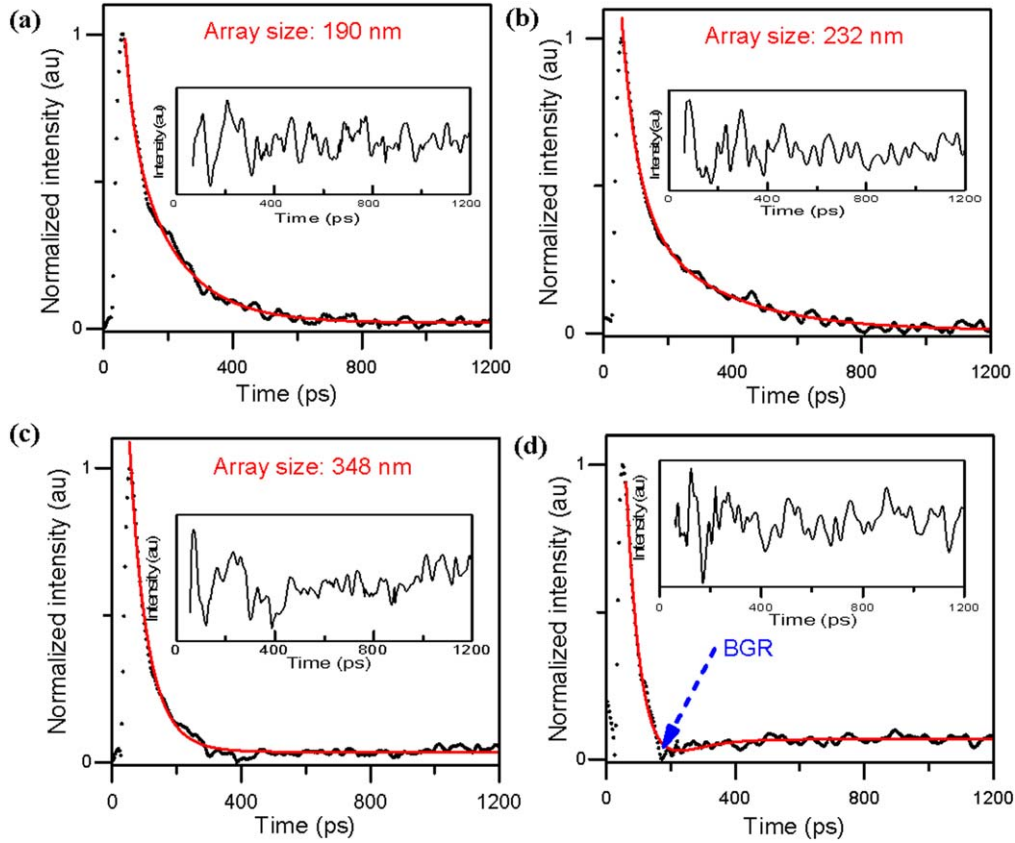
Figure 3. (a)–(c) Show the differential reflection ($-\Delta R/R$) signal of 2.9% doped GZO nanoparticle arrays (black dots) and their fitting (red continuous line). Their sizes are listed along. While (d) is the 348 nm nanoparticle array of the undoped sample which reveals the BGR effect. Inserts: the differential reflection after removal of background contribution.

Ga concetrations, which shows the oscillation frequency reduces with increase in doping. The peak frequencies were 30.4 GHz, 28.5 GHz, 24.0 GHz and 19.3 GHz for GZO films with different Ga concentrations of 0%, 2.9%, 5% and 7.3%, respectively. Using Thomsen's model, the oscillation frequency can be expressed as follow [46, 47]:

$$f = \frac{n v k_{\text{probe}}}{\pi},\qquad(4)$$

where $k_{\text{probe}} = 2\pi/\lambda$ is the wave number of probe beam ($\lambda = 800$ nm), n is the refractive index, and $v = 6200$ ms^{-1} is the sound velocity of ZnO [19]. A refractive index value of 1.97 is obtained, which is close to the reported value of 1.9597 [48]. And we analyze the FFT signals peaks in figure 5(a) (see the insert in figure 5(a)). The peak frequencies follow the expected eigen modes frequency sequence $f_m = m(v/2d)$, with $m = 1, 2, 3\ldots\ldots$ and v is the longitudinal sound velocity and d the nano-film thickness which is $\sim$90 nm. So we confirm that the oscillation is attributed to an acoustic pulse generated at the film surface and travelling back and forth across the surface. The acoustic phonon frequencies of the material is a factor of the material properties according to the elasticity theory ($v\alpha\sqrt{E/\rho}$) where E is the Young's modulus and ρ is the mass density [49]. Though the Ga impurity changes the ρ, it is unlikely to significantly influence the frequency of the vibrations alone because the

difference between the Zn and Ga atom mass is small (factor of 1.0664). Another factor which can also affect the frequency of the oscillation is the atomic radius difference. The difference in the atomic radius leads to lattice distortions [36] and influence on the phonon velocity and refractive index [50].

Interestingly, the plots of the frequency and internal strain against the doping concentration clearly show the relationship between them (figure 5(b)). Whereas the frequency showed a decrease as the doping level was increased, the opposite was for the internal strain. Since the frequency varies proportionally to E and inversely proportionally to ε, it can be concluded that the reduction of the oscillation frequency could be attributed to the increased strain as a result of doping. Generally, the acoustic phonons play a dominant role in heat transport and thermoelectric properties of semiconductor nanostructures; therefore it is interesting to assess its implication of doping. Kargar *et al* [50] explained the relationship between the scattering rates ($1/\tau$, where τ is the phonon lifetime) and the introduction of dopants at low temperature where the Umklapp scattering is minimal. They showed $1/\tau$ was proportional to the concentration of foreign atoms, atomic radius and mass of the host and foreign atoms. This fundamentally implies that the introduction of Ga dopants could alter the thermal conductivity of the ZnO by changing the scattering rates. Thus, in GZO nanoparticles, similar crystal structure distortion and strain will be
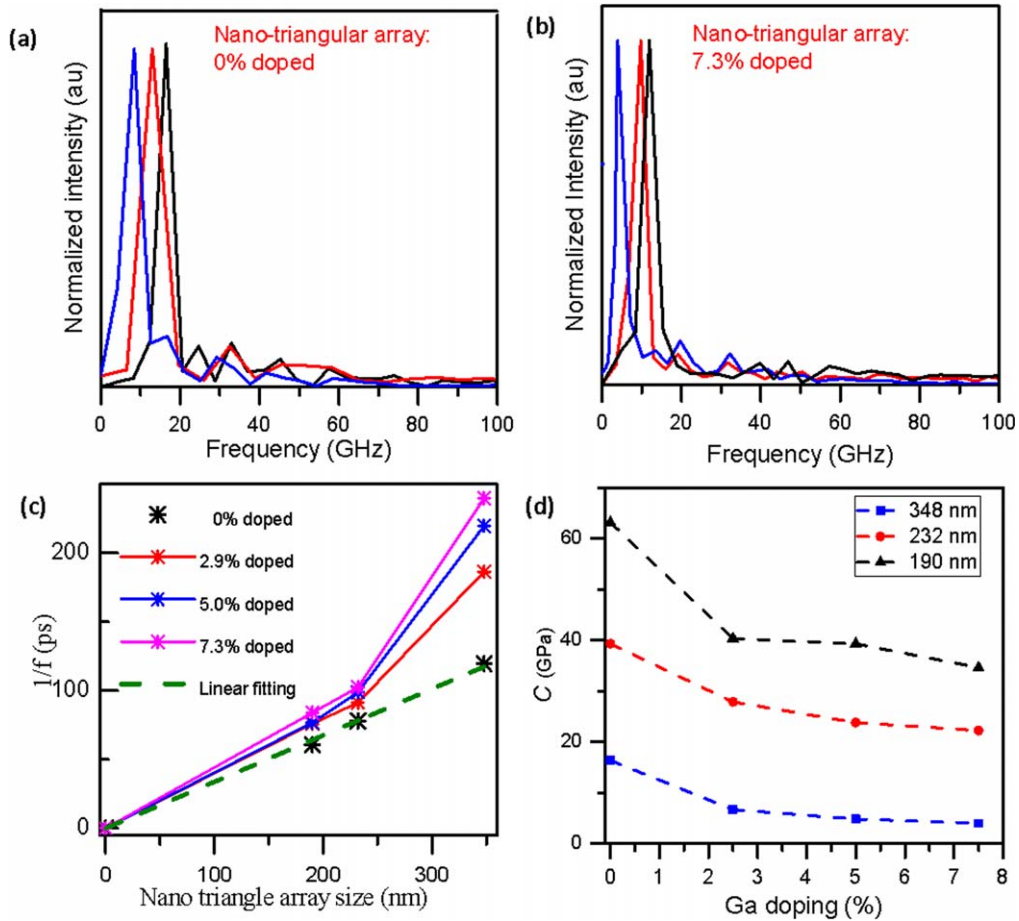
Figure 4. (a) and (b) show fast Fourier transform of the acoustic vibration in GZO nano-particle arrays of undoped and 7.3% Ga concentration respectively. The bisector lengths of the arrays are: 190 nm, 232 nm and 348 nm in black, red and blue respectively. (c) Shows the relationship between the acoustic vibration and the nano-particle arrays size at various doping concentrations. The dotted line shows the linear fitting for the 0% GZO nano-particle arrays. (d) Shows the variation of the elasticity (*C*) with doping at different Ga doping levels.
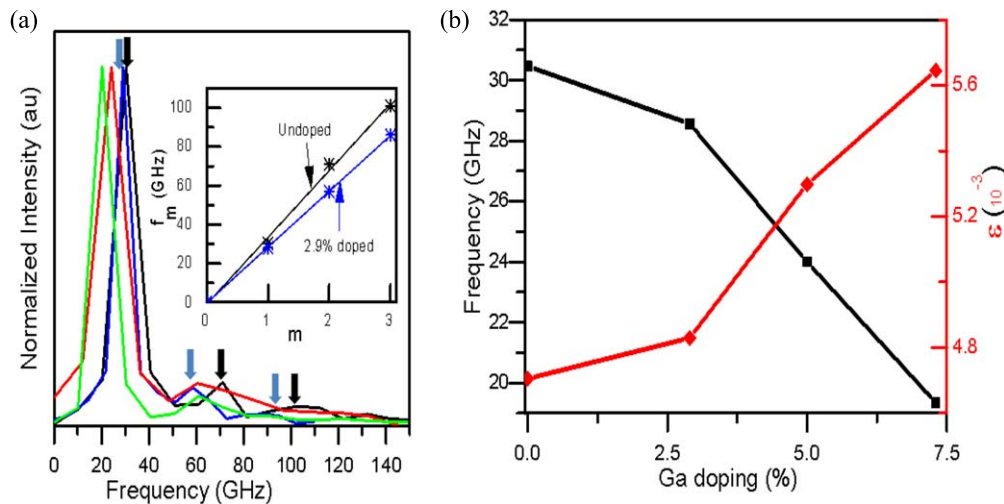
Figure 5. (a) FFT of the acoustic phonons oscillation (black-0%, blue-2.9%, red-5% and green-7.3% doped). Insert, breathing frequency oscillation modes of undoped and doped GZO (b) relationship between the oscillation frequency peak and the internal strain introduced as a result of Ga doping.

introduced by Ga doping. This could alter the thermal conductivity of GZO nanoparticles, which can affect the vibration phonons frequency.

4. Conclusion

In summary, the dynamic properties of the charge carriers and the acoustic vibration in GZO nanoparticles were studied by using pump-probe experiments with varying the Ga doping concentration. The acoustic vibration frequency excited in the GZO nanoparticles of the same size decreased as the doping concentration increased, which was attributed to the internal strain in the crystal introduced by doping. Additionally, the oscillation period in GZO nanoparticles shows nonlinear increase as the size is increased, which is different from the linear increase on sizes in undoped ZnO particles. The results are helpful for evaluating the crystal structure distortion and elastic characteristics of doped nano-materials with optical methods.

Acknowledgments

ORCID iDs

Dickson Mwenda Kinyua ● https://orcid.org/0000-0001-5436-3518
Hua Long ● https://orcid.org/0000-0002-7959-7828
Stephen Njoroge ● https://orcid.org/0000-0002-0861-0095

References

[1] Prasanth R, Van Vugt L K, Vanmaekelbergh D A M and Gerritsen H C 2006 Resonance enhancement of optical second harmonic generation in a ZnO nanowire *Appl. Phys. Lett.* **88** 181501

[2] Geren K, Liu S W, Zhou H J, Zhang Y, Tian R and Xiao M 2009 Second-order susceptibilities of ZnO nanorods from forward second-harmonic scattering *J. Appl. Phys.* **105** 063531

[3] Polyakov A Y, Smirnov N B, Govorkov A V, Kozhukhova E A, Pearton S J, Norton D P, Osinsky A and Dabiran A 2006 Electrical properties of undoped bulk ZnO substrates *J. Electron. Mater.* **35** 663–9

[4] Lu T-C, Lai Y-Y, Lan Y-P, Huang S-W, Chen J-R, Wu Y-C, Hsieh W-F and Deng H 2012 Room temperature polariton lasing versus photon lasing in a ZnO-based hybrid microcavity *Opt. Express* **20** 5530–7

[5] Hoffmann S P, Albert M, Weber N, Sievers D, Förstner J, Zentgraf T and Meier C 2018 Tailored UV emission by nonlinear IR excitation from ZnO photonic crystal nanocavities *ACS Photonics* **5** 1933–42

[6] Peng W, Qu S, Cong G and Wang Z 2006 Synthesis and temperature-dependent near-band-edge emission of chain-like Mg-doped ZnO nanoparticles *Appl. Phys. Lett.* **88** 101902

[7] Ng Z-N, Chan K-Y, Muslimin S and Knipp D 2018 P-Type characteristic of nitrogen-doped ZnO Films *J. Electron. Mater.* **47** 5607–13

[8] Balaprakash V, Gowrisankar P, Sudha S and Rajkumar R 2018 Aluminum doped ZnO transparent conducting thin films prepared by sol-gel dip coating technique for solar cells and optoelectronic applications *Mater. Technol.* **33** 414–20

[9] Wang R, Sleight A W and Cleary D 1996 High conductivity in gallium-doped zinc oxide powders *Chem. Mater.* **8** 433–9

[10] Maeng W and Park J-S 2013 Growth characteristics and film properties of gallium doped zinc oxide prepared by atomic layer deposition *J. Electroceram.* **31** 338–44

[11] Yang Q, Zhang X, Zhou X and Liang S 2017 Growth of Ga-doped ZnO films by thermal oxidation with gallium and their optical properties *AIP Adv.* **7** 055106

[12] Ratcliff E L, Sigdel A K, Macech M R, Nebesny K, Lee P A, Ginley D S, Armstrong N R and Berry J J 2012 Surface composition, work function, and electrochemical characteristics of gallium-doped zinc oxide *Thin Solid Films* **520** 5652–63

[13] Habeeb A A, Long H, Bao L, Wang K, Wang B and Lu P 2016 Surface plasmonic resonances and enhanced IR spectra in GZO nano-triangle arrays *Mater. Lett.* **172** 36–9

[14] Ko Y-D, Kim K-C and Kim Y-S 2012 Effects of substrate temperature on the Ga-doped ZnO films as an anode material of organic light emitting diodes *Superlattices Microstruct.* **51** 933–41

[15] Cabanillas-Gonzalez J, Grancini G and Lanzani G 2011 Pump-probe spectroscopy in organic semiconductors: monitoring fundamental processes of relevance in optoelectronics *Adv. Mater.* **23** 5468–85

[16] Cheng T, Vidal J, Zeiger H, Dresselhaus G, Dresselhaus M and Ippen E 1991 Mechanism for displacive excitation of coherent phonons in Sb, Bi, Te, and Ti$_2$O$_3$ *Appl. Phys. Lett.* **59** 1923–5

[17] Kini R, Kent A, Stanton N and Henini M 2006 Generation and detection of terahertz coherent transverse-polarized acoustic phonons by ultrafast optical excitation of Ga As/Al As superlattices *Appl. Phys. Lett.* **88** 134112

[18] Ge S, Liu X, Qiao X, Wang Q, Xu Z, Qiu J, Tan P-H, Zhao J and Sun D 2014 Coherent longitudinal acoustic phonon approaching THz frequency in multilayer molybdenum disulphide *Sci. Rep.* **4** 5722

[19] Lin J-H, Shen Y-K, Liu W-R, Lu C-H, Chen Y-H, Chang C-P, Lee W-C, Hong M, Kwo J-R and Hsu C-H 2016 Coherent acoustic phonon oscillation accompanied with backward acoustic pulse below exciton resonance in a ZnO epifilm on oxide-buffered Si (1 1 1) *J. Phys. D: Appl. Phys.* **49** 325102

[20] Liu W, Xie W, Guo W, Xu D, Hu T, Ma T, Yuan H, Wu Y, Zhao H and Shen X 2014 Coherent scattering of exciton polaritons and acoustic phonons in a ZnO single crystal *Phys. Rev.* B **89** 201201

[21] Ayouch A, Dieudonne X, Vaudel G, Piombini H, Valle K, Gusev V, Belleville P and Ruello P 2012 Elasticity of an assembly of disordered nanoparticles interacting via either van der waals-bonded or covalent-bonded coating layers *ACS Nano* **6** 10614–21

[22] Ruello P, Ayouch A, Vaudel G, Pezeril T, Delorme N, Sato S, Kimura K and Gusev V E 2015 Ultrafast acousto-plasmonics in gold nanoparticle superlattices *Phys. Rev.* B **92** 174304

[23] Crut A, Maioli P, Del Fatti N and Vallée F 2015 Acoustic vibrations of metal nano-objects: time-domain investigations *Phys. Rep.* **549** 1–43

[24] Gandolfi M, Crut A, Medeghini F, Stoll T, Maioli P, Vallee F, Banfi F and Del Fatti N 2018 Ultrafast thermo-optical dynamics of plasmonic nanoparticles *J. Phys. Chem.* C **122** 8655–66

[25] Taubert R, Hudert F, Bartels A, Merkt F, Habenicht A, Leiderer P and Dekorsy T 2007 Coherent acoustic oscillations of nanoscale Au triangles and pyramids: influence of size and substrate *New J. Phys.* **9** 376

[26] Stoll T, Maioli P, Crut A, Rodal-Cedeira S, Pastoriza-Santos I, Vallée F and Del Fatti N 2015 Time-resolved investigations of the cooling dynamics of metal nanoparticles: impact of environment *J. Phys. Chem.* C **119** 12757–64

[27] Chen H-P, Wu Y-C, Mante P A, Tu S-J, Sheu J-K and Sun C-K 2012 Femtosecond excitation of radial breathing mode in 2D arrayed GaN nanorods *Opt. Express* **20** 16611–7

[28] Chen J, Wang K, Long H, Han X, Hu H, Liu W, Wang B and Lu P 2018 Tungsten disulfide-gold nanohole hybrid metasurfaces for nonlinear metalenses in the visible region *Nano Lett.* **18** 1344–50

[29] Babar A R, Deshamukh P R, Deokate R J, Haranath D, Bhosale C H and Rajpure K Y 2008 Gallium doping in transparent conductive ZnO thin films prepared by chemical spray pyrolysis *J. Phys. D: Appl. Phys.* **41** 135404

[30] Liu J, Zhang W, Song D, Ma Q, Zhang L, Zhang H, Ma X and Song H 2014 Gallium-doped zinc oxide targets fabricated by sintering: impact of target quality on sputtered thin film properties *Mater. Sci. Semicond. Process.* **27** 1–11

[31] Htwe Z M, Zhang Y-D, Yao C-B, Li H and Yuan P 2017 Ultrafast carrier dynamics and third order nonlinear optical properties of aluminum doped zinc oxide (AZO) thin films *Opt. Mater.* **66** 580–8

[32] Muchuweni E, Sathiaraj T S and Nyakotyo H 2016 Effect of gallium doping on the structural, optical and electrical properties of zinc oxide thin films prepared by spray pyrolysis *Ceram. Int.* **42** 10066–70

[33] Ishioka K, Petek H, Kaydashev V E, Kaidashev E M and Misochko O V 2010 Coherent optical phonons of ZnO under near resonant photoexcitation *J. Phys.: Condens. Matter* **22** 465803

[34] Liu W-R, Lin J-H, Chen J-S, Cheng H-M, Li S-J, Chen H-R, Hsu C-H and Hsieh W-F 2018 Saturation and beating of acoustic phonon oscillations excited near the exciton resonance of strained polar ZnO/Zn 0.8 Mg 0.2 O multiple quantum wells *RSC Adv.* **8** 7980–7

[35] Ou P-C, Lin J-H, Chang C-A, Liu W-R and Hsieh W-F 2010 Thickness effect on ultrafast thermalization of carriers in above-band-gap states in ZnO epitaxial films *J. Phys. D: Appl. Phys.* **43** 495103

[36] Zou Y S, Yang H, Wang H P, Lou D, Tu C J and Zhang Y C 2013 Microstructure, optical and photoluminescence properties of Ga-doped ZnO films prepared by pulsed laser deposition *Physica* B **414** 7–11

[37] Miao X, Zhang G, Wang F, Yan H and Ji M 2018 Layer-dependent ultrafast carrier and coherent phonon dynamics in black phosphorus *Nano Lett.* **18** 3053–9

[38] Liu W, Li X, Song Y, Zhang C, Han X, Long H, Wang B, Wang K and Lu P 2018 Cooperative enhancement of two-photon-absorption-induced photoluminescence from a 2D perovskite-microsphere hybrid dielectric structure *Adv. Funct. Mater.* **28** 1707550

[39] Shi J, Ma H, Ma G, Ma H and Shen J 2008 Structure and ultrafast carrier dynamics in n-type transparent Mo: ZnO nanocrystalline thin films *Appl. Phys.* A **92** 357–60

[40] Campos A, Arbouet A, Martin J, Gerard D, Proust J, Plain J and Kociak M 2017 Plasmonic breathing and edge modes in aluminum nanotriangles *ACS Photonics* **4** 1257–63

[41] Huang W Y, Qian W and El-Sayed M A 2005 The optically detected coherent lattice oscillations in silver and gold monolayer periodic nanoprism arrays: the effect of interparticle coupling *J. Phys. Chem.* B **109** 18881–8

[42] Hu M, Petrova H, Wang X and Hartland G V 2005 Time-resolved and steady state spectroscopy of polydisperse colloidal silver nanoparticle samples *J. Phys. Chem.* B **109** 14426–32

[43] Poyser C L, Czerniuk T, Akimov A, Diroll B T, Gaulding E A, Salasyuk A S, Kent A J, Yakovlev D R, Bayer M and Murray C B 2016 Coherent acoustic phonons in colloidal semiconductor nanocrystal superlattices *ACS Nano* **10** 1163–9

[44] Kucheyev S O, Bradby J E, Williams J S, Jagadish C and Swain M V 2002 Mechanical deformation of single-crystal ZnO *Appl. Phys. Lett.* **80** 956–8

[45] Coleman V A, Bradby J E, Jagadish C, Munroe P, Heo Y W, Pearton S J, Norton D P, Inoue M and Yano M 2005 Mechanical properties of ZnO epitaxial layers grown on *a*- and *c*-axis sapphire *Appl. Phys. Lett.* **86** 203105

[46] Thomsen C, Grahn H T, Maris H J and Tauc J 1986 Surface generation and detection of phonons by picosecond light pulses *Phys. Rev.* B **34** 4129

[47] Mante P-A, Lehmann S, Anttu N, Dick K A and Yartsev A 2016 Nondestructive complete mechanical characterization of zinc blende and wurtzite GaAs nanowires using time-resolved pump-probe spectroscopy *Nano Lett.* **16** 4792–8

[48] Bond W L 1965 Measurement of the refractive indices of several crystals *J. Appl. Phys.* **36** 1674–7

[49] Su M-N *et al* 2017 Optomechanics of single aluminum nanodisks *Nano Lett.* **17** 2575–83

[50] Kargar F, Penilla E H, Aytan E, Lewis J S, Garay J E and Balandin A A 2018 Acoustic phonon spectrum engineering in bulk crystals via incorporation of dopant atoms *Appl. Phys. Lett.* **112** 191902